An Adaptive Inpainting Algorithm Based on DCT Induced Wavelet Regularization

Yan-Ran Li, Lixin Shen, and Bruce W. Suter

***Abstract*—In this work, we propose an image inpainting optimization model whose objective function is a smoothed ℓ^1 norm of the weighted non-decimated discrete cosine transform (DCT) coefficients of the underlying image. By identifying the objective function of the proposed model as a sum of a differentiable term and a non-differentiable term, we give a basic algorithm inspired by Beck and Teboulle's recent work [1] for the model. Based on this basic algorithm, we propose an automatic way to determine the weights involved in the model and update them in each iteration. The discrete cosine transform as an orthogonal transform is used in various applications. We view the rows of a discrete cosine transform matrix as the filters associated with a multiresolution analysis. Non-decimated wavelet transforms with these filters are explored to analyze images to be inpainted. Our numerical experiments verify that under the proposed framework, the filters from a discrete cosine transform matrix demonstrate promise for the task of image inpainting.**

***Index Terms*—Discrete Cosine Transform, Framelet, Moreau envelope, Inpainting, ℓ^1 minimization.**

I. Introduction

In many applications, only partial data are available in an image due to a variety of reasons including impulsive noise caused by malfunctioning pixels in camera sensors, faulty memory locations in hardware, transmission in a noisy channel, text or signature superposed on an image, and a scratch in a picture [2], [3]. Recovery of missing pixels is called image inpainting, an active area of research in image processing. Applications of image inpainting include old film restoration, video inpainting [4], de-interlacing of video sequences [5], and cloud removal from remotely sensed images [6]. Restoring missing pixels becomes indispensable in the above applications.

Many successful algorithms for image inpainting have been developed in the past decade. These inpainting algorithms can be roughly classified into three groups: geometric partial differential equation (PDE), patch, and sparse representation based ones. Classical, yet popular, methods for image inpainting use PDEs and variational formulations to propagate available image information from observed domains into missing regions as a way of smoothly transporting the contours of the image into the regions being inpainted [3], [7], [8], [9], [10], [11], [12]. Within the category of PDE-based methods, there are a number of approaches which perform well for piecewise smooth images with sharp edges. Patch-based (or exemplar-based) inpainting methods fill in missing pixels of an image from known non-local observed data by exploring local repetitions of local information. Recent work in this direction includes [13], [14], [15], [16], [17] and the references therein. Algorithms in this category propagate the known patches into missing patches gradually in a fashion of cut-and-paste, and perform well, especially for missing regions with texture and large sizes. Sparse representation for image inpainting was recently addressed in [18], [19], [20], [21], [22], [23], [24], [25], [26], [27], [28], and the references therein. The main idea of these algorithms is to sparsely represent an image by a redundant system which is formed by a set of transforms such as the discrete cosine transform, wavelets, framelets, and curvelets. The missing pixels are then inferred by shrinking coefficients adaptively and iteratively from this sparse representation.

In this paper, we propose an inpainting method which could be viewed as a sort of combination of a variational approach and a sparse representation based approach. The proposed inpainting method is developed based upon an optimization model whose objective functional is a smoothed ℓ_1 norm of the coefficients of the underlying image under a given redundant system. The redundant system is generated from the discrete cosine transform (DCT) matrix of second type [29]. More precisely, we identify the rows of a given DCT matrix as the filters associated with a multiresolution analysis which is referred to as the DCT-Haar wavelet system in the following discussion. The non-decimated transform using the DCT-Haar wavelet filters yields a redundant system that is used in our model. We show that this redundant system incorporated with the proposed model performs particularly well for inpainting images with incomplete information. We propose an adaptive inpainting algorithm to solve the proposed model. We also propose a way to automatically tune the parameters appearing in our algorithm.

The remainder of this paper is organized as follows. In Section II, we begin with reviewing several variational inpainting models based on sparse representations. We then propose our model for inpainting which is regularized by DCT-Haar wavelets. In Section III, we develop an adaptive iterative algorithm for solving the proposed model. Numerical experiments for the proposed algorithm are presented in Section IV. Our conclusions are drawn in Section V.

II. An Inpainting Model Regularized by DCT-Haar Wavelets

Our inpainting model is formulated as an optimization problem in which the variational objective functional has a

The work of L. Shen was supported by the US National Science Foundation under grant DMS-0712827 and DMS-1115523 and by the 2011 Air Force Summer Faculty Fellowship Program

regularization term formed by a sparse representation of the underlying image. We point out that the proposed optimization model is connected with the reweighted ℓ^1 minimization model [30], but with several distinct and promising properties.

We begin with introducing some notation used in the following. Let f_{org} the original image be defined on the domain $\Omega = \{1, 2, \ldots, n\}$ and a nonempty proper subset $\mathcal{D}$ of Ω be given. The observed image g is modeled as

$$g[k] = \begin{cases} f_{org}[k], & k \in \Omega \setminus \mathcal{D}; \\ h[k], & k \in \mathcal{D}, \end{cases} \tag{1}$$

where $h[k]$ with $k \in \mathcal{D}$ could represent any types of degradations to the original image including impulsive noise and texts superposed on f_{org}.

Associated with the sets Ω and $\mathcal{D}$, we define an $n \times n$ diagonal matrix, denoted by $P_{\mathcal{D}}$, whose k-th diagonal entry is 1 if $k \in \Omega \setminus \mathcal{D}$ and 0 if $k \in \mathcal{D}$. The goal of image inpainting is to seek an image f such that $P_{\mathcal{D}} f = P_{\mathcal{D}} g$ while f can truthfully retain original information of f_{org}.

Prior to introducing our variational model for image inpainting, we review some sparse representation based image inpainting models which are most related to ours.

A. A Brief Review of Three Inpainting Models

The first example among these models is the morphological component analysis based simultaneous cartoon and texture image inpainting [18]. The minimization task in [18] is

$$\{f_c^\star, f_t^\star\} = \underset{f_c, f_t}{\operatorname{argmin}} \left\{ \frac{1}{2}\|P_{\mathcal{D}}(g - f_c - f_t)\|_2^2 + \lambda\|W_c f_c\|_1 + \lambda\|W_t f_t\|_1 + \gamma\|f_c\|_{TV} \right\}, \tag{2}$$

where λ and γ are positive regularization parameters, W_c is a redundant system leading to sparse representations for cartoon-like images, W_t is a redundant system able to represent texture-like images sparsely, and $\|\cdot\|_{TV}$ is the total variation. The image $f_c^\star + f_t^\star$ will be the inpainted outcome. A work similar to the one in [18] was also formulated in [22].

The second example is from [31], [20], [23] using tight framelets. The corresponding minimization task is

$$x^\star = \underset{x}{\operatorname{argmin}} \left\{ \frac{1}{2}\|P_{\mathcal{D}}(g - W^\top x)\|_2^2 + \frac{1}{2}\|(\mathrm{Id} - WW^\top)x)\|_2^2 + \|\Gamma x\|_1 \right\}, \tag{3}$$

where W is a tight framelet system with $W^\top W = \mathrm{Id}$ and Γ is a diagonal matrix with non-negative diagonal components. The inpainted image reads as $P_{\mathcal{D}} g + (\mathrm{Id} - P_{\mathcal{D}})W^\top x^\star$. The numerical experiments in [31], [20], [23] showed that model (3) is particularly suitable for cartoon-like images.

The third example from [28] is an extension of the first two examples for tackling images having both cartoon and texture contents. The proposed model is

$$\{x_c^\star, x_t^\star\} = \underset{x_c, x_t}{\operatorname{argmin}} \left\{ \frac{1}{2}\|P_{\mathcal{D}}(g - \sum_{k\in\{c,t\}} W_k^\top x_k)\|_2^2 + \frac{1}{2}\sum_{k\in\{c,t\}} \|(\mathrm{Id} - W_k W_k^\top)x_k)\|_2^2 + \sum_{k\in\{c,t\}} \|\Gamma_k x_k\|_1 \right\}, \tag{4}$$

where W_c and W_t are framelet systems favoring cartoon and texture contents of images, respectively, Γ_c and Γ_t are diagonal matrices with non-negative diagonal components. The inpainted image resulting from model (4) is $P_{\mathcal{D}} g + (\mathrm{Id} - P_{\mathcal{D}})(W_c^\top x_c^\star + W_t^\top x_t^\star)$.

The success of models (2) and (4) fully relies on the selection of appropriate redundant systems W_c and W_t. The rationale of choosing desirable W_c and W_t is that W_c should yield sparse representations for the cartoon parts of the underlying image while W_t should yield sparse representations for the texture parts of the image. However, two issues arise from using models (2) and (4). The first issue is that there is a lack of precise mathematical definitions of cartoon and texture components of an image. This leads to a difficulty in separating an image exactly into its cartoon part and texture part. Hence, it affects the choice of appropriate systems W_c and W_t. The second issue is that the regularization parameter λ in (2) and the diagonal matrices Γ_c and Γ_t in (4) are essential, but should be pre-determined. An automatic way of determining λ, Γ_c and Γ_t is not available yet. Both issues need to be addressed if models (2) and (4) are adopted for image inpainting.

Instead of directly addressing the aforementioned two issues, we take a different point of view about image inpainting. As usual, we infer each missing pixel on $\mathcal{D}$ using the known information from its neighborhood. Our approach is to choose a redundant system associated with a multiresolution analysis such that the filters from the multiresolution analysis has the ability to extract information from neighborhoods of pixels with different sizes. The candidates of redundant systems are associated with multiresolution analysis generated from the DCTs that will be presented in detail in the following subsection.

B. DCT-Haar Multiresolution Analysis

Discrete cosine transforms are frequently used orthogonal transforms in applied mathematics and engineering [29]. Among various types of the DCTs, the discrete cosine transform of second type (DCT-II) is the most popular one of all and will be chosen below in our discussion.

The standard $m \times m$ DCT-II matrix C is given by

$$C := \frac{1}{\sqrt{m}} \left[\epsilon_k \cos \frac{(k-1)(2j-1)\pi}{2m} : k, j = 1, 2, \ldots, m \right],$$

where $\epsilon_1 = 1$ and $\epsilon_k = \sqrt{2}$ for $k = 2, 3, \ldots, m$. The matrix C is orthogonal, i.e., $C^\top C = I$. Denoting by c_k the k-th row of $\frac{1}{\sqrt{m}} C$, we can directly verify that the sum of entries of c_k is 1 for $k = 1$ and zero for $k = 2, 3, \ldots, m$. Hence, the vector c_1 can be viewed as a low-pass filter while the others can be viewed as high-pass filters. In particular, when $m = 2$,

c_1 and c_2 are low-pass and high-pass filters corresponding to the well-known Haar multiresolution analysis. Indeed, c_1 and c_k, $k = 2, 3, \ldots, m$, from a general $m \times m$ DCT-II matrix, are the low-pass and high-pass filters associated with a multiresolution analysis of dilation m, which is called the DCT-Haar multiresolution analysis in the following discussion.

We denote by P_k the matrix representation of the filters c_k, $k = 1, 2, \ldots, m$, under a proper boundary condition. For a simple exposition, we adopt the periodic condition for the construction of the P_k in this paper. In this scenario, P_k is a size of $\ell \times \ell$ circulant matrix with $\begin{bmatrix} c_k & 0_{1\times(\ell-m)} \end{bmatrix}$ as its first row. For such the matrices P_k, we have the following result.

Proposition 1: Let C be the $m \times m$ DCT-II matrix and c_k be the k-th row of $\frac{1}{\sqrt{m}}C$. Then we have that

$$\sum_{k=1}^{m} P_k^\top P_k = \mathrm{Id}.$$

Proof: Let us denote by p_k the first column of the matrix P_k, for $k = 1, 2, \ldots, m$. From the orthogonality of C, we have that

$$\sum_{k=1}^{m} p_k^2[\beta] = \begin{cases} \frac{1}{m}, & \text{if } \beta = 1 \text{ or } \beta > \ell - m + 1; \\ 0, & \text{otherwise.} \end{cases} \quad (5)$$

$$\sum_{k=1}^{m} p_k[\beta] p_k[\tau] = 0 \quad \text{for all} \quad 1 \le \beta < \tau \le \ell. \quad (6)$$

Let U be the $\ell \times \ell$ Fourier transform matrix, i.e., $U := \frac{1}{\sqrt{\ell}}[\exp(-\frac{2\pi(\alpha-1)(\beta-1)i}{\ell}) : \alpha, \beta = 1, 2, \ldots, \ell]$. Since any circulant matrix can be diagonalized by the Fourier transform matrix, we have that

$$\sum_{k=1}^{m} P_k^\top P_k = \ell U^* \left(\sum_{k=1}^{m} \mathrm{diag}(U^* p_k) \mathrm{diag}(U p_k) \right) U.$$

By the equation $U^*U = \mathrm{Id}$, we just need to show $\sum_{k=1}^{m} \mathrm{diag}(U^* p_k)\mathrm{diag}(U p_k) = \frac{1}{\ell}\mathrm{Id}$. It suffices to prove that $\sum_{k=1}^{m} |(U^* p_k)[\alpha]|^2 = \frac{1}{\ell}$ for each $\alpha \in \{1, 2, \ldots, \ell\}$. Let us denote by u_α the αth column of U. Note that $|(U^* p_k)[\alpha]|^2 = p_k^\top u_\alpha u_\alpha^* p_k = \sum_{\beta=1}^{\ell} |u_\alpha[\beta]|^2 p_k^2[\beta] + 2\sum_{1\le\beta<\tau\le\ell} \mathrm{Re}(u_\alpha[\beta] u_\alpha^*[\tau]) p_k[\beta] p_k[\tau]$. Summing this equation for k from 1 to m, interchanging the order of the summations $\sum_{k=1}^{m}$ with $\sum_{\beta=1}^{\ell}$ and $\sum_{1\le\beta<\tau\le\ell}$, and using equations (5)-(6) together with the fact of $|u_\alpha[\beta]| = \frac{1}{\sqrt{\ell}}$ for all α and β, we get that $\sum_{k=1}^{m} |(U^* p_k)[\alpha]|^2 = \frac{1}{\ell}$. This completes the proof. ∎

For a given one-dimensional vector $x \in \mathbb{R}^\ell$, the vector $P_k x$ is the non-decimated DCT-Haar wavelet coefficients of x produced by the filter c_k. From the coefficients $P_k x$, $k = 1, 2, \ldots, m$, the vector x can be perfectly reconstructed from $P_k x$ due to Proposition 1.

The two dimensional DCT-Haar multiresolution analysis, constructed by the one dimensional DCT-Haar multiresolution analysis through the tensor product technique, will be used to represent images. The matrices $Q_1 := P_1 \otimes P_1$ and $Q_{(i-1)m+j} = P_i \otimes P_j$ with $i, j = 1, 2, \ldots, m$ and $(i, j) \neq (1, 1)$ are, respectively, the low-pass and high-pass filters associated with the two dimensional DCT-Haar multiresolution analysis. Here, the symbol $\otimes$ denotes matrix tensor product. For an $\ell \times \ell$ image x, we can view it as a vector (denoted it by x again) in $\mathbb{R}^n$ with $n = \ell^2$ by concatenating its columns. The vectors $Q_k x$, $k = 1, 2, \ldots, m^2$, are the non-decimated DCT-Haar wavelet coefficients of x and satisfy the perfect reconstruction formula, i.e., $x = \sum_{k=1}^{m^2} Q_k^\top Q_k x$.

With these matrices Q_k, we form a matrix W of the size $m^2 n \times n$ as follows

$$W := [Q_1^\top, Q_2^\top, \ldots, Q_{m^2}^\top]^\top. \quad (7)$$

By Proposition 1, we have the perfect reconstruction condition for the matrices Q_k, that is, $W^\top W = \mathrm{Id}$. Therefore, W is a tight framelet transform matrix.

C. The Proposed Inpainting Model

The proposed inpainting model with a redundant system W generated from the DCT-II is as follows:

$$\min_{f,d} \left\{ \frac{1}{2}\|Wf - d\|_2^2 + \|\Gamma d\|_1 : P_{\mathcal{D}} f = P_{\mathcal{D}} g \right\}, \quad (8)$$

where Γ is a diagonal matrix with non-negative diagonal components and d is an auxiliary vector.

Let us explain model (8) in detail. The requirement $P_{\mathcal{D}} f = P_{\mathcal{D}} g$ says that the solution to be found should interpolate the observed data g exactly on the set $\Omega \setminus \mathcal{D}$, in other words, the solution of model (8) is in the set

$$\mathcal{C} := \{f : f \in \mathbb{R}^n \quad \text{and} \quad P_{\mathcal{D}} f = P_{\mathcal{D}} g\}, \quad (9)$$

which is convex. In the set $\mathcal{C}$, the solution f to be sought is sparse in the sense that its transformed coefficients Wf are close to a sparse vector d with respect to the weight matrix Γ.

Model (8) can be written into a compact and unconstrained form by using the notion of an indicator function and the Moreau envelope in convex analysis. The indicator function $\iota_{\mathcal{C}}$ on the convex set $\mathcal{C}$ is defined as

$$\iota_{\mathcal{C}}(f) := \begin{cases} 0, & \text{if } f \in \mathcal{C}; \\ +\infty, & \text{otherwise.} \end{cases}$$

Then, the objective functional in model (8) becomes

$$\min_{f,d} \left\{ \frac{1}{2}\|Wf - d\|_2^2 + \|\Gamma d\|_1 + \iota_{\mathcal{C}}(f) \right\}. \quad (10)$$

Next, for a proper convex function φ defined on $\mathbb{R}^{m^2 n}$, that is, $\varphi : \mathbb{R}^{m^2 n} \to \mathbb{R} \cup \{+\infty\}$, having a non-empty domain (the set on which φ is finite), the Moreau envelope [32] of φ, denoted by env_φ, is a function from $\mathbb{R}^{m^2 n}$ to $\mathbb{R}$, defined for a given $u \in \mathbb{R}^{m^2 n}$ by

$$\mathrm{env}_\varphi(u) := \min_v \left\{ \frac{1}{2}\|u - v\|_2^2 + \varphi(v) \right\}.$$

By identifying Wf, d , and $\|\cdot\|_1 \circ \Gamma$ in (10) as u, v, and φ, respectively, in the definition of the Moreau envelope, model (8) is written as

$$\min_f \left\{ \mathrm{env}_{\|\cdot\|_1 \circ \Gamma}(Wf) + \iota_{\mathcal{C}}(f) \right\}. \quad (11)$$

As reported in many research articles (e.g. [18], [22], [33]), the DCT-Haar multiresolution analysis is suitable for representing images rich in texture information. We would like

to demonstrate that the DCT-Haar multiresolution analysis is also suitable for representing images rich in cartoon information provided that the resulting coefficients of the underlying image are properly modified and an appropriate nonlinear reconstruction approach is used. To this end, we illustrate this point by a numerical example portrayed in Figure 1. An algorithm for model (11) will be developed in section III while more examples will be provided in section IV. Figure 1(a) is an original cartoon image while Figure 1(b) is the cartoon image overlaid with text. The inpainted images shown in Figure 1(c)-(f) with the peak signal-to-noise ratio (PSNR) values of 37.38dB, 37.37dB, 37.04dB and 39.96dB are, respectively, from three competing algorithms, namely, spline framelets (SF) based on [20], spline framelet and local DCT (SF-LDCT) based on [28], and morphological component analysis (MCA) based on [18], and our proposed algorithm. We can see that the quality of the image in Figure 1(f) is better than those images in Figure 1(c)-(e) in terms of visual perception.

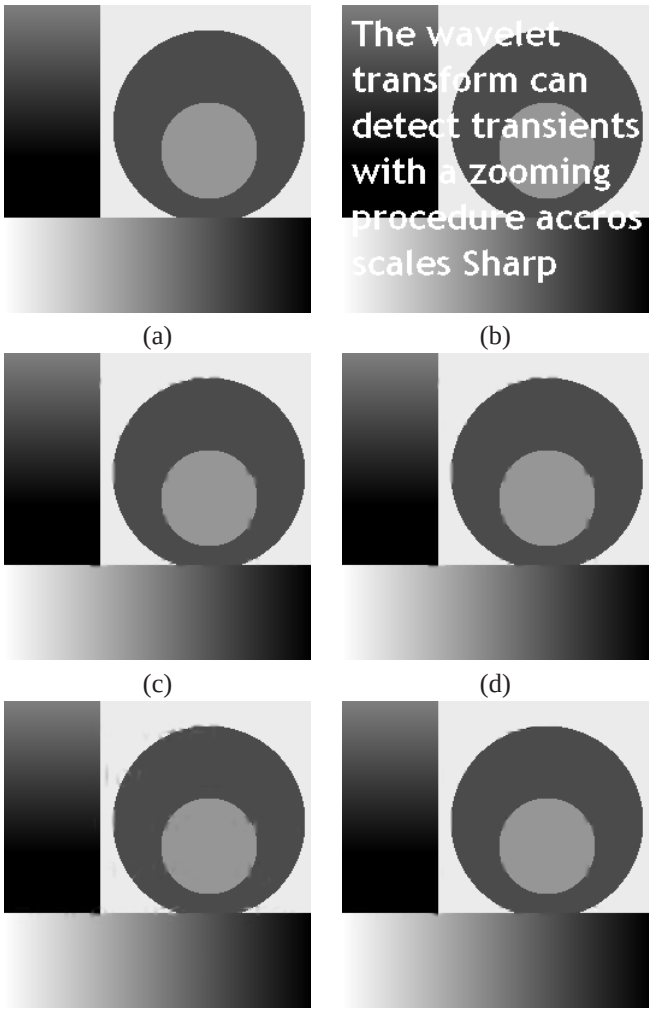

Fig. 1. Performance of various inpainting algorithms for a cartoon image with text. (a) the original test image; (b) the test image with text; inpainted images by (c) SF (PSNR=37.38 dB); (d) SF-LDCT (PSNR=37.37 dB); (e) MCA (PSNR=37.04 dB); and (f) the proposed algorithm (PSNR=39.96 dB), respectively.

In the rest of this section, we make a connection between model (11) and the weighted ℓ^1 minimization model for sparse signal recovery in [30].

D. Model (11) *vs. A Weighted* ℓ^1 *Minimization Model*

The problem discussed in [30] is to determine an object $x_0 \in \mathbb{R}^q$ from the data $y = \Phi x_0$, where Φ is a $n \times q$ matrix with $n < q$. Under the sparsity assumption on the vector x_0 which we wish to recover, it is common in compressive sensing to solve the combinatorial optimization problem

$$\min_{x\in\mathbb{R}^q} \|x\|_0 \quad \text{subject to} \quad y = \Phi x, \tag{12}$$

where $\|x\|_0$ is the number of non-zero elements of x. It is well known that the optimization problem (12) is nonconvex and generally impossible to solve. A common alternative is to replace $\|x\|_0$ in problem (12) by $\|x\|_1$. As a result, it converts the nonconvex optimization problem to a convex one. Surprisingly, under an appropriate condition on the relation between the number of observations n and the number of elements q of a sparse data x, the optimization based on the ℓ^1 model can exactly recover sparse signals and closely approximate compressible signals with high probability [34]. The use of the ℓ^1 norm in sparse signal recovery has been well understood and justified (see, e.g., [35], [36] and the references therein).

Motivated by the observation that larger coefficients are penalized more heavily in the ℓ^1 norm than smaller coefficients, unlike the more democratic penalization of the ℓ^0 norm, it was proposed in [30] to consider the "weighted" ℓ^1 optimization problem

$$\min_{x\in\mathbb{R}^q} \|Tx\|_1 \quad \text{subject to} \quad y = \Phi x, \tag{13}$$

where T is a diagonal matrix with positive numbers $t[1], t[2], \ldots, t[q]$ on its diagonal. In [30], a heuristic way was suggested to solve the problem (13) as follows: (i) beginning with the initialized weight matrix $T^{(0)}$ of all 1's on its diagonal; (ii) solving $x^{(\ell)} = \operatorname{argmin}_{x\in\mathbb{R}^q} \|T^{(\ell)}x\|_1$ subject to $y = \Phi x$; (iii) updating the weights $t^{(\ell+1)}[k] := (|x^{(\ell)}[k]| + \epsilon)^{-1}$ for $k = 1, 2, \ldots, q$ and a given positive number ϵ; and (iv) terminating on convergence or ℓ attaining a specified maximum number of iterations; otherwise incrementing ℓ and going to step (ii). We remark that the convergence analysis of this algorithm is analyzed recently in [37].

Our proposed model (11) is in the sprit of (13), but with several additional promising properties. Let us explain it now in detail. Define $x := Wf$, $y := P_{\mathcal{D}}g$, and $\Phi := P_{\mathcal{D}}W^\top$, where W is of size $q \times n$. We consider a problem of seeking a set of coefficients x that synthesizes the signal $f = W^\top x$ as follows:

$$\min_x \operatorname{env}_{\|\cdot\|_1\circ\Gamma}(x) \quad \text{subject to} \quad y = \Phi x, \tag{14}$$

which is identical to problem (11) when W is an orthogonal system. By the definition of the Moreau envelope, a direct calculation gives, for a nonnegative number a,

$$\operatorname{env}_{a|\cdot|}(u) = \begin{cases} a|u| - \frac{1}{2}a^2, & \text{if } |u| \geq a; \\ \frac{1}{2}|u|^2, & \text{otherwise.} \end{cases} \tag{15}$$

Since Γ is an $n\times n$ diagonal matrix with non-negative diagonal elements, then $\|\cdot\|_1\circ\Gamma$ is separable. Hence $\mathrm{env}_{\|\cdot\|_1\circ\Gamma}(x) = \sum_{k=1}^{q}\mathrm{env}_{\gamma[k]|\cdot|}(x[k])$. Further, by using formula (15), we define a diagonal matrix T with diagonal elements as

$$t[k] := \begin{cases} \gamma[k]\left(\frac{2|x[k]|-\gamma[k]}{2|x[k]|}\right), & \text{if } |x[k]|\geq\gamma[k];\\ \frac{1}{2}|x[k]|, & \text{otherwise.}\end{cases} \tag{16}$$

With this weight matrix T, we have that $\mathrm{env}_{\|\cdot\|_1\circ\Gamma}(x) = \|Tx\|_1$. This is the reason why we call Γ the weight matrix as well. By comparing the formulation (14) together with (16) to that of (13), one can view (14) as a weighted ℓ^1 minimization problem. The strategy in determining the weight T is obviously different from the one given in [30]. In Step (iii) of the aforementioned approach in [30], the weight corresponding to an entry of a sparse signal is simply the reversal of the sum of the magnitude of the entry and a small positive number ϵ. The weight for an entry of a sparse signal in (16) is determined by a pre-determined threshold, i.e., the matrix Γ that will be estimated in an automatic way in the next section. On the other hand, unlike the objective functional in (13), the one in (14) is differentiable and its gradient is Lipschitz continuous. This property is particularly important in developing a fast and efficient numerical algorithm for solving the optimization problem (14). Again, this will be illustrated in the next section.

III. Algorithms

In this section, we propose an iterative algorithm for solving model (11) which involves a redundant system W generated from the DCT and a weight matrix Γ. We further suggest a variant of the algorithm with a varying weight matrix Γ in iterations.

A. Algorithm for Model (11)

This subsection presents a fast algorithm for solving model (11). The cost function of the model is the sum of the functions $\mathrm{env}_{\|\cdot\|_1\circ\Gamma}\circ W$ and $\iota_{\mathcal{C}}$. By the definition of indicator function, $\iota_{\mathcal{C}}$ is not differentiable. We will show that $\mathrm{env}_{\|\cdot\|_1\circ\Gamma}\circ W$ is differentiable and its gradient is Lipschitz continuous. Hence, Beck and Teboulle's gradient descent method known as accelerated proximal descent gradient (APDG) algorithm [1] is suitable for solving model (11).

The accelerated proximal gradient algorithm is developed for a general nonsmooth convex optimization model

$$\min_f\{\psi(f)+\phi(f)\}, \tag{17}$$

where $\phi:\mathbb{R}^n\to\mathbb{R}\cup\{+\infty\}$ is a convex function, $\psi:\mathbb{R}^n\to\mathbb{R}$ is continuously differentiable with Lipschitz continuous gradient $L(\psi)$, i.e., $\|\nabla\psi(f_1)-\nabla\psi(f_2)\|_2\leq L(\psi)\|f_1-f_2\|_2$ for every $f_1,f_2\in\mathbb{R}^n$. The corresponding APDG algorithm proposed in [1] is given in Algorithm 1.

Algorithm 1 (Accelerated proximal decent gradient (APDG)):

1) set $\tau_1=1$, $f_0=P_{\mathcal{D}}g+(\mathrm{Id}-P_{\mathcal{D}})X$, where X is a matrix whose entries are uniformly distributed on the interval $[0,255]$;
2) Take $u_1=f_0$ and $L=L(\psi)$ as a Lipschitz constant of $\nabla\psi$;
3) For $k=1,2,\ldots$, compute
   a) $f_k = \mathrm{argmin}_f\{\phi(f)+\frac{L}{2}\|f-\big(u_k-\frac{1}{L}\nabla\psi(u_k)\big)\|_2^2\}$
   b) $\tau_{k+1}=\frac{1+\sqrt{1+4\tau_k^2}}{2}$
   c) $u_{k+1}=f_k+\left(\frac{\tau_k-1}{\tau_{k+1}}\right)(f_k-f_{k-1})$

To apply APDG Algorithm 1 for model (11), we need to identify the corresponding functions ψ and ϕ in model (11). To this end, we give some properties of the functions $\mathrm{env}_{\|\cdot\|_1\circ\Gamma}\circ W$ and $\iota_{\mathcal{C}}$ in model (11).

Lemma 1: If Γ is a diagonal matrix with nonnegative diagonal entries and W is the tight framelet transform matrix given in (7), then $\mathrm{env}_{\|\cdot\|_1\circ\Gamma}\circ W$ is continuously differentiable and its gradient is Lipschitz continuous with the Lipschitz constant 1.

Proof: It is well-known that the Moreau envelope of any function is always differentiable and the gradient of the Moreau envelope is Lipschitz continuous with Lipschitz constant 1 [32], [38]. Thus, the chain rule yields $\nabla(\mathrm{env}_{\|\cdot\|_1\circ\Gamma}\circ W)=W^\top\nabla\mathrm{env}_{\|\cdot\|_1\circ\Gamma}\circ W$. Therefore, for any f_1 and f_2 in $\mathbb{R}^n$, we have that

$$\begin{aligned}\|\nabla(\mathrm{env}_{\|\cdot\|_1\circ\Gamma}\circ W)(f_1)-\nabla(\mathrm{env}_{\|\cdot\|_1\circ\Gamma}\circ W)(f_2)\|_2\\ \leq\|W^\top\|_2\|W\|_2\|f_1-f_2\|_2.\end{aligned}$$

Notice that $\|W^\top\|_2^2=\|W\|_2^2=\|W^\top W\|_2=1$ due to $W^\top W=\mathrm{Id}$. Hence, the Lipschitz constant of the gradient $\nabla(\mathrm{env}_{\|\cdot\|_1\circ\Gamma}\circ W)$ is 1. This completes the proof. ■

The following result explains how to compute $\nabla\mathrm{env}_{\|\cdot\|_1\circ\Gamma}$.

Lemma 2: If Γ is an $n\times n$ diagonal matrix with nonnegative diagonal entries, then the kth entry, $k=1,2,\ldots,n$, of the gradient of $\mathrm{env}_{\|\cdot\|_1\circ\Gamma}$ at $f\in\mathbb{R}^n$ is

$$\nabla\mathrm{env}_{\|\cdot\|_1\circ\Gamma}(f)[k]=\begin{cases}\gamma_k\mathrm{sign}(f[k]), & \text{if } |f[k]|\geq\gamma_k;\\ f[k], & \text{otherwise,}\end{cases}$$

where γ_k is the kth diagonal entry of Γ.

Proof: Since Γ is a diagonal matrix with nonnegative diagonal elements, then we have that $\mathrm{env}_{\|\cdot\|_1\circ\Gamma}(f)=\sum_{k=1}^{n}\mathrm{env}_{|\gamma_k\cdot|}(f[k])$. Hence, the conclusion of the lemma follows immediately from (15). ■

Lemma 3: If g, as shown in (1), is an image to be inpainted on the domain $\mathcal{D}$ and the convex set $\mathcal{C}$ is given in (9), then for any $\alpha>0$ and $f\in\mathbb{R}^n$ we have that

$$P_{\mathcal{D}}g+(\mathrm{Id}-P_{\mathcal{D}})f=\mathrm{argmin}_u\left\{\frac{\alpha}{2}\|u-f\|_2^2+\iota_{\mathcal{C}}(u)\right\} \tag{18}$$

Proof: By the definition of the indicator function, we know that

$$\frac{\alpha}{2}\|u-f\|_2^2+\iota_{\mathcal{C}}(u)=\begin{cases}\frac{\alpha}{2}\|u-f\|_2^2, & \text{if } u\in\mathcal{C};\\ +\infty, & \text{otherwise.}\end{cases}$$

Because $P_{\mathcal{D}}(\mathrm{Id}-P_{\mathcal{D}})=0$, then $\|u-f\|_2^2=\|P_{\mathcal{D}}(u-f)\|_2^2+\|(\mathrm{Id}-P_{\mathcal{D}})(u-f)\|_2^2\geq\|P_{\mathcal{D}}(g-f)\|_2^2$ for any $u\in\mathcal{C}$. The equality in the above holds when we choose $u=P_{\mathcal{D}}g+(\mathrm{Id}-P_{\mathcal{D}})f$. This completes the proof. ■

With Lemmas 1 and 3, we identity the functions $\mathrm{env}_{\|\cdot\|_1\circ\Gamma}\circ W$ and $\iota_{\mathcal{C}}$ in model (11) as ψ and ϕ in model (17), respectively. By using Lemmas 1-3, an algorithm based on APDG for model (11) is proposed in Algorithm 2.

Algorithm 2 (Algorithm for Model (11)*):*

1) set $\tau_1=1$, $f_0=P_{\mathcal{D}}g+(\mathrm{Id}-P_{\mathcal{D}})X$, where X is a matrix whose entries are uniformly distributed on the interval $[0,255]$, and a pre-determined matrix Γ;
2) Take $u_1=f_0$;
3) For $k=1,2,\ldots$, compute
   a) $f_k = P_{\mathcal{D}}g+(\mathrm{Id}-P_{\mathcal{D}})(u_k - W^\top\nabla\mathrm{env}_{\|\cdot\|_1\circ\Gamma}(Wu_k))$
   b) $\tau_{k+1}=\frac{1+\sqrt{1+4\tau_k^2}}{2}$
   c) $u_{k+1}=f_k+\left(\frac{\tau_k-1}{\tau_{k+1}}\right)(f_k-f_{k-1})$

Let $\{f_k\}$ be the sequence generated by Algorithm 2. Then all elements in the sequence are in $\mathcal{C}$. Let $f^\star$ be the point at which the function $\mathrm{env}_{\|\cdot\|_1\circ\Gamma}(Wf)+\iota_{\mathcal{C}}(f)$ in model (11) achieves its minimal value. Then $f^\star$ must be in $\mathcal{C}$ as well. For Algorithm 2, the rate of convergence of the sequence of function values $\mathrm{env}_{\|\cdot\|_1\circ\Gamma}(Wf_k)$ to the optimal value $\mathrm{env}_{\|\cdot\|_1\circ\Gamma}(Wf^\star)$ is given as follows:

$$\mathrm{env}_{\|\cdot\|_1\circ\Gamma}(Wf_k)-\mathrm{env}_{\|\cdot\|_1\circ\Gamma}(Wf^\star)\leq\frac{2\|f_k-f^\star\|_2^2}{(k+1)^2}$$

for all $k\geq 1$. The proof of the above estimate is given in [1].

The remaining problem for Algorithm 2 is how to choose the matrix Γ. We plan to use the procedure proposed in our recent work [39] to automatically estimate Γ associated with evaluating $\mathrm{env}_{\|\cdot\|_1\circ\Gamma}(Wu)$ for an input image u. To this end, let us denote by v the Wu. For any non-negative integer p and positive integer q, we denote by $\mathrm{quot}\,(p,q)$ and $\mathrm{rem}\,(p,q)$ the quotient and the remainder, respectively, when p is divided by q. For the ℓth entry of v, we can identify this entry by the triplets (ℓ_1,ℓ_2,ℓ_3) where $\ell_1=\mathrm{quot}(\mathrm{quot}(\ell-1,n),m)+1$, $\ell_2=\mathrm{rem}(\mathrm{quot}(\ell-1,n),m)+1$, and $\ell_3=\mathrm{rem}(\ell-1,n)+1$. The pair of indexes (ℓ_1,ℓ_2) indicates that $v[\ell]$ the ℓth entry of v is from the subband generated by $P_{\ell_1}\otimes P_{\ell_2}$ and the index ℓ_3 indicates that this entry $v[\ell]$ is the ℓ_3th entry of the vector $Q_{(\ell_1-1)m+\ell_2}u=(P_{\ell_1}\otimes P_{\ell_2})u$. With this notation, as suggested in [39], γ_ℓ the ℓth entry of Γ is estimated as follows:

$$\gamma_\ell=\begin{cases}0, & \text{if } 1\leq\ell\leq n;\\ \frac{\sqrt{2}\sigma_u^2}{m^2\sigma_{v[\ell]}}, & \text{otherwise,}\end{cases}\tag{19}$$

where σ_u^2 is the noise variance of the image u and $\sigma_{v[\ell]}^2$ is the variance of $v[\ell]$ with the assumption of $v[\ell]$ being Laplace distributed. Here, $\sigma_{v[\ell]}^2$ can be estimated by [40], [39]

$$\sigma_{v[\ell]}^2=\max\left\{\left[\sum_{k\in\mathfrak{R}(v[\ell])}\frac{\sqrt{2}|v[k]|}{|\mathfrak{R}(v[\ell])|}\right]^2-\sigma_u^2/m^2,10^{-6}\right\},$$

Fig. 2. The test images superposed by "Text 1" (the first column) and "Text 2" (the second column). The square region in each image is the part of the corresponding image zoomed in.

where the index set $\mathfrak{R}(v[\ell])$ is the neighborhood of the coefficient $v[\ell]$ in the corresponding (ℓ_1,ℓ_2) subband and $|\mathfrak{R}(v[\ell])|$ is the cardinality of the set $\mathfrak{R}(v[\ell])$. The window $\mathfrak{R}(v[\ell])$ of size $(m+2)\times(m+2)$ is adopted in our experiments.

Based on the formula (19), Algorithm 3 is presented as a variant of Algorithm 2 with adaptive updating the matrix Γ in iterations.

Algorithm 3 (Adaptive Algorithm for Model (11)*):*

1) Set $\tau_1=1$, $f_0=P_{\mathcal{D}}g+(\mathrm{Id}-P_{\mathcal{D}})X$, where X is a matrix whose entries are uniformly distributed on the interval $[0,255]$, and a pre-given positive integer s;
2) Take $u_1=f_0$;
3) For $k=1,2,\ldots$, compute
   a) Estimate Γ_k from the input image $u_{k'}$ based on (19) with $k'=s\cdot\mathrm{quot}\,(k-1,s)+1$
   b) $f_k = P_{\mathcal{D}}g+(\mathrm{Id}-P_{\mathcal{D}})(u_k - W^\top\nabla\mathrm{env}_{\|\cdot\|_1\circ\Gamma_k}(Wu_k))$
   c) $\tau_{k+1}=\frac{1+\sqrt{1+4\tau_k^2}}{2}$
   d) $u_{k+1}=f_k+\left(\frac{\tau_k-1}{\tau_{k+1}}\right)(f_k-f_{k-1})$

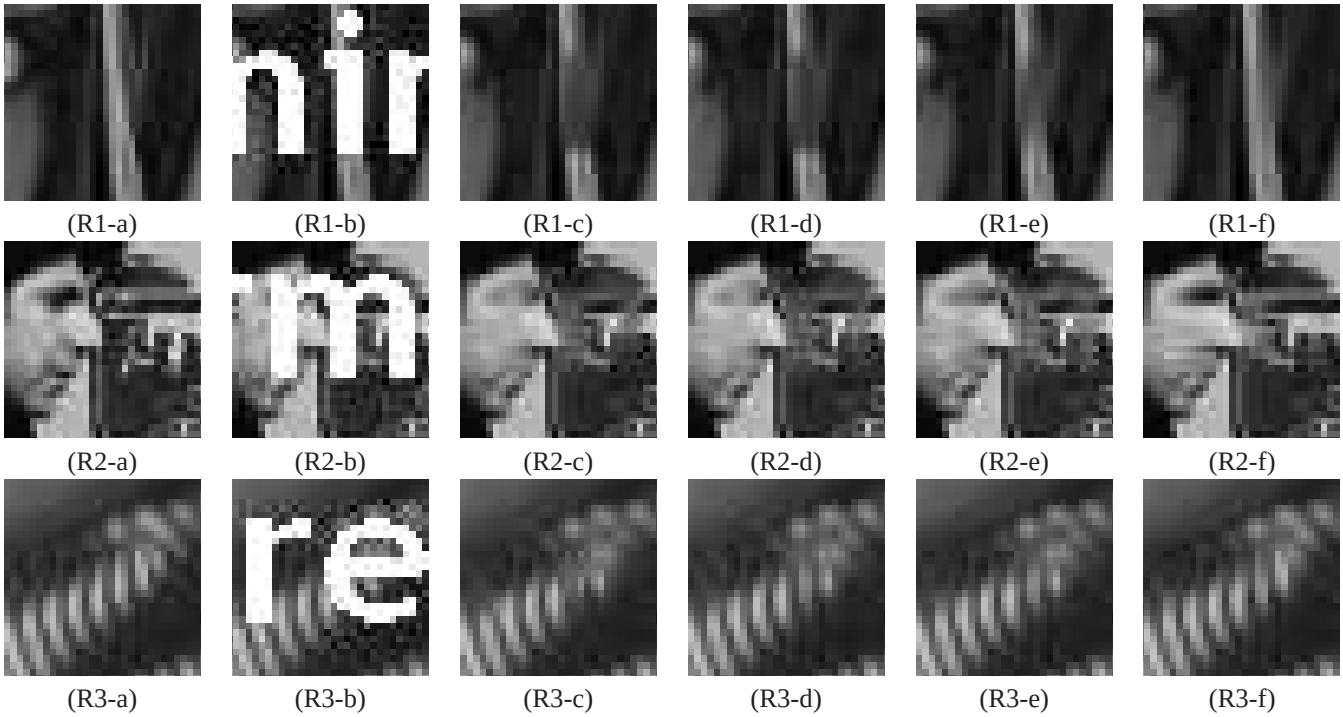

Fig. 3. Column 1: Zoomed-in portions of the original test images; Column 2: Zoomed-in portions of the original test images with "Text 1"; Columns 3-6 are inpainted images by using SF, SF-LDCT, MCA, and Algorithm 3, respectively.

We remark that γ_ℓ being zeros for $1 \leq \ell \leq n$ implies that the scaling coefficients of Wu_k (i.e., $Q_1 u_k$) in Step 3(a) of Algorithm 3 will be unmodified. Furthermore, the matrices Γ_k, for k running from $s(q-1)+1$ to sq with q being a natural number, are identical and are estimated from the $u_{s(q-1)+1}$ via (19). In other words, the matrices Γ_k are updated only once for every s iterations. In particular, if $s = 1$, the matrices Γ_k will be updated at each iteration.

IV. Experiments

In this section, we present numerical results to demonstrate the performance of our proposed inpainting algorithm. We shall compare results of the proposed algorithm to those of three state-of-the-art methods in the literature.

In our numerical experiments, three test images are "Lena", "Cameraman", and "Barbara" with a size of 256×256. Three benchmark schemes are used in our experiments: Spline Framelet based (SF) [20], Spline Framelet and Local DCT based (SF-LDCT) [28], and Morphological Component Analysis based (MCA) [18]. The implementations of all three algorithms are provided by their own authors. Our proposed algorithm in the experiments is Algorithm 3 which is essentially parameter-free. In the spirit of reproducible research, the Matlab source codes of the proposed Algorithm 3 can be obtained by sending an email to `lshen03@syr.edu`. Each algorithm is carried out until the stopping condition $\|f_{k+1} - f_k\|_2^2 / \|f_k\|_2^2 < 7.5 \times 10^{-4}$ is satisfied. The quality of the inpainted images is evaluated in terms of the peak signal-to-noise ratio (PSNR) defined by

$$\mathrm{PSNR} = 10 \log_{10} \frac{255^2 n}{\|f_{restored} - f_{org}\|_2^2} (\mathrm{dB}),$$

where $f_{restored}$ is the restored image and f_{org} is the original image each with a total of n pixels.

This section contains three subsections. In the first two subsections, the scenarios for text removal and random impulsive noise removal will be discussed. The last subsection is about the effect of choosing the DCT-Haar multiresolution analysis of various dilations m.

A. Experimental Results on Text Removal

Removing texts superposed on images is a typical problem in image inpainting. Two text documents named as "Text 1" and "Text 2" are overlying on the test images shown in the first column and the second column of Figure 2, respectively. The words in "Text 2" are thicker and denser than that in "Text 1". A set consisting the locations of the words in "Text 1" and "Text 2" serves as the set $\mathcal{D}$.

The first experiment tests numerically the choice of the number s in Algorithm 3 in terms of the CPU time that the algorithm consumed and the PSNR values of the inpainted images for text removal. We observe from Table I that the algorithm with s being 1 and 8 performs comparably in terms of the PSNR values of the inpainted images, but the algorithm with $s = 8$ uses much less the CPU time than that with $s = 1$. Hence, in what follows, we always choose $s = 8$ for Algorithm 3.

As expected, for each algorithm, the inpainted image for an image with "Text 1" should be better than that with "Text 2" in terms of PSNR values. This can be clearly observed from Table II. By comparing the performance of Algorithm 3 with the other methods SF, SF-LDCT, and MCA, the PSNR values listed in Table II indicate that Algorithm 3 is the best in terms

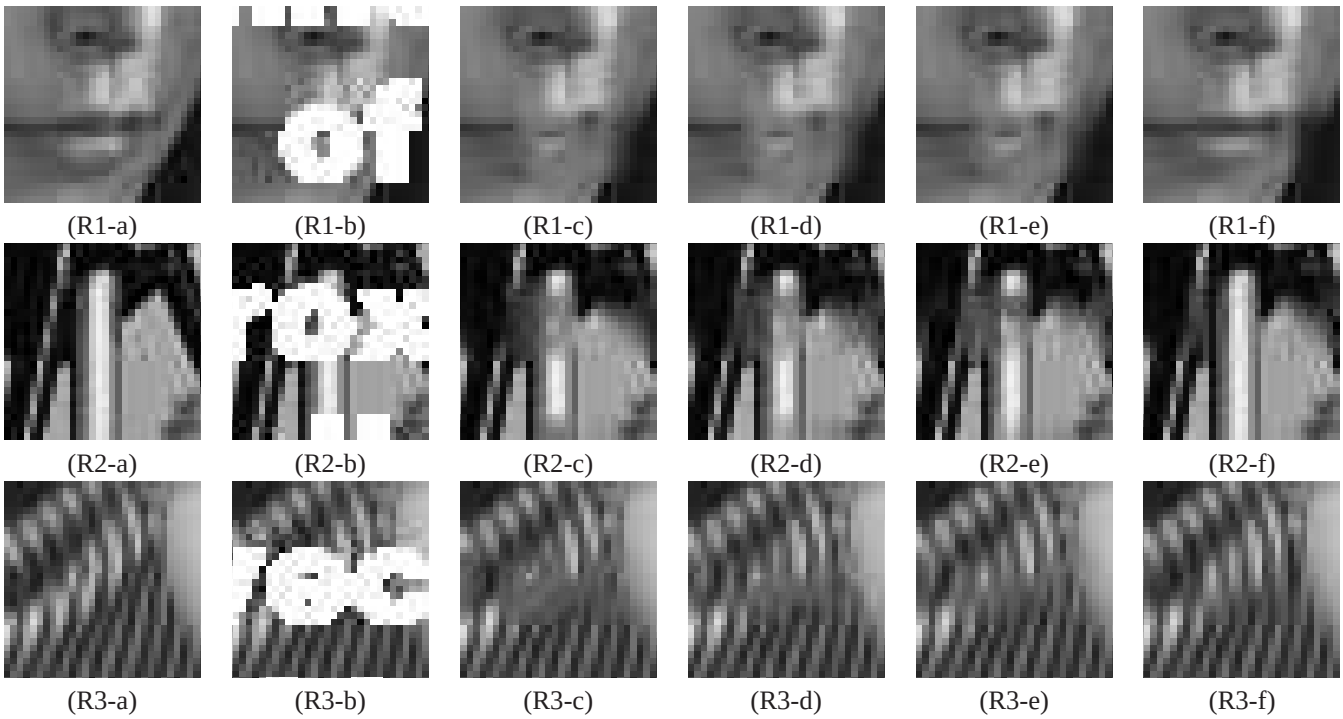

Fig. 4. Column 1: Zoomed-in portions of the original test images; Column 2: Zoomed-in portions of the original test images with "Text 2"; Columns 3-6 are inpainted images by using SF, SF-LDCT, MCA, and Algorithm 3, respectively.

TABLE I
THE PAIR $(\cdot,\cdot)$ REPRESENTS THE PSNR VALUE OF THE INPAINTED IMAGES AND THE CPU TIME (SECONDS) USED FOR TEXT REMOVAL BY ALGORITHM 3 WITH THE PARAMETER s BEING 1 AND 8, RESPECTIVELY.

s	"Lena"	"Cameraman"	"Barbara."	Case
1	(34.16, 203)	(31.96, 213)	(37.15, 162)	"Text 1"
8	(33.95, 76)	(31.96, 81)	(36.98, 64)	
1	(29.41, 446)	(28.55, 368)	(30.37, 438)	"Text 2"
8	(29.31, 144)	(28.60, 135)	(30.12, 142)	

of PSNR values. We further point it out that the CPU times consumed by both Algorithm 3 and the MCA are comparable for all tested cases.

TABLE II
THE PAIR $(\cdot,\cdot)$ REPRESENTS THE PSNR VALUE OF AN INPAINTED IMAGE AND THE CPU TIME (SECONDS) USED BY SF, SF-LDCT, MCA, AND ALGORITHM 3 FOR TEXT REMOVAL.

Algorithms	"Lena"	"Cameraman"	"Barbara."	Case
SF	(32.12, 143)	(30.29, 151)	(32.81, 127)	
SF-LDCT	(31.73, 260)	(30.58, 282)	(35.22, 266)	"Text 1"
MCA	(32.48, 92)	(30.63, 88)	(35.37, 89)	
Algorithm 3	(33.95, 76)	(31.96, 81)	(36.98, 64)	
SF	(28.36, 228)	(26.78, 221)	(27.79, 183)	
SF-LDCT	(28.10, 425)	(26.83, 426)	(29.27, 415)	"Text 2"
MCA	(28.20, 109)	(26.47, 110)	(29.25, 123)	
Algorithm 3	(29.31, 144)	(28.60, 135)	(30.12, 142)	

Let us have a closer look at the visual quality of the inpainted images by various algorithms. When "Text 1" is overlying on the test images, the zoomed-in portions of the inpainted images are depicted in Figure 3. One can see that Algorithm 3 can efficiently remove the superposed words over the regions having both cartoon and texture components (see Figure 3(R1-f)-(R3-f)). Those words are identifiable in the inpainted images by the other three methods (see columns 3, 4, and 5 of Figure 3). We can draw the same conclusion for the images having "Text 2". The corresponding results are shown in Figure 4.

B. Experimental Results on Random Impulsive Noise Removal

The problem of removing random impulsive noise can be viewed as one of image inpainting. We can adopt the adaptive median filter [41] to locate the pixels of images corrupted by random impulsive noise. The detected locations form a set $\mathcal{D}$ which is the region of an image to be inpainted and therefore is assumed to be known in our experiments. Three impulsive noise levels, namely 30%, 50%, and 70%, are used to test robustness and efficiency of the proposed algorithm. The experimental results with SF, SF-LDCT, MCA, and Algorithm 3 are reported in Table III. As we can observe from this table, the improvements made by Algorithm 3 over the other three algorithms in terms of PSNR values are up to 5.31 dB, which is significant.

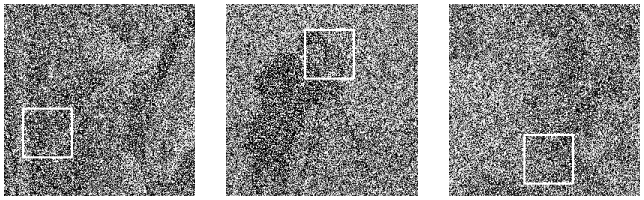

Fig. 5. The images of "Lena", "Cameraman", and "Barbara" (from left to right) corrupted by impulsive noise with noise level of 70%.

The visual comparisons of the inpainted images by SF, SF-LDCT, MCA, and Algorithm 3 are presented for the images of "Lena", "Cameraman", and "Barbara" corrupted by impulsive

Fig. 6. The inpainted images for the images of “Lena”, “Cameraman”, and “Barbara” (from top to bottom) corrupted by impulsive noise with noise level of 70%. The results (from left to right) are produced by SF, SF-LDCT, MCA, and Algorithm 3, respectively.

TABLE III
THE PAIR $(\cdot,\cdot)$ REPRESENTS THE PSNR VALUE OF THE INPAINTED IMAGES AND THE CPU TIME (SECONDS) USED FOR BY SF, SF-LDCT, MCA, AND ALGORITHM 3 FOR REMOVING RANDOM IMPULSIVE NOISE.

Algorithm	“Lena”	“Cameraman”	“Barbara”	Case
SF	(28.44, 316)	(25.45, 303)	(26.13, 264)	
SF-LDCT	(27.69, 577)	(25.23, 540)	(28.37, 559)	70%
MCA	(27.85, 92)	(25.02, 91)	(29.11, 92)	
Algorithm 3	(28.72, 90)	(26.13, 102)	(30.35, 95)	
SF	(31.34, 205)	(28.92, 198)	(29.77, 185)	
SF-LDCT	(30.70, 372)	(28.24, 356)	(32.60, 320)	50%
MCA	(31.09, 84)	(28.37, 90)	(32.67, 85)	
Algorithm 3	(32.35, 62)	(29.97, 74)	(35.08, 57)	
SF	(34.96, 147)	(32.50, 150)	(34.49, 142)	
SF-LDCT	(34.01, 246)	(31.55, 251)	(37.30, 264)	30%
MCA	(35.33, 106)	(32.19, 106)	(37.99, 108)	
Algorithm 3	(36.50, 50)	(33.60, 56)	(39.33, 43)	

noise with noise level of 70%. Figure 5 shows the noisy “Lena”, “Cameraman”, and “Barbara” images while Figure 6 presents the inpainted images using these four algorithms. It can be observed that all the algorithms can inpaint the images well, but Algorithm 3 is the best of them in terms of the inpainted images (see the last column in Figure 6) having less ringing artifacts than the ones by SF-LDCT and MCA (see the second and third columns in Figure 6) and having a more fruitful texture than the one by SF (see the first column in Figure 6).

For a further visual comparison, we present the results for the zoomed-in portions of the images shown in Figure 6. These results with our proposed algorithm together with other three competing algorithms are provided in Figure 7. We can see that our proposed algorithm retrieves fine structures of the original images very well and yields the inpainted images with good visual quality. The zoomed-in portion of the “Lena” image (see, Figure 7(R1-e)) displays a part of Lena’s hair and a part of her hat. The hair and edges of the hat in the inpainted images in Figure 7(R1-a)-(R1-c), which are from SF, SF-LDCT, and MCA, respectively, are blurry with some white and black spots. In a contrast, the hair and edges of the hat in Figure 7(R1-d) from Algorithm 3 are more focused. For the image of “Cameraman”, the right ear of the Cameraman (see Figure 7(R2-e)) is distinguishable in Figure 7(R2-d) by Algorithm 3, but are not clear in the inpainted images in Figure 7(R2-a)-(R2-c), which are from SF, SF-LDCT, and MCA, respectively. The face of the Cameraman with Algorithm 3 looks smoother than the ones with the other three algorithms. The shapes of the camera in Figure 7(R2-b) and (R2-d) are closer to the original shape in Figure 7(R2-e) than the ones in Figure 7(R2-a) and (R2-c). The “Barbara” image having both texture and cartoon components is considered as a good example in image inpainting. The head scarf of the

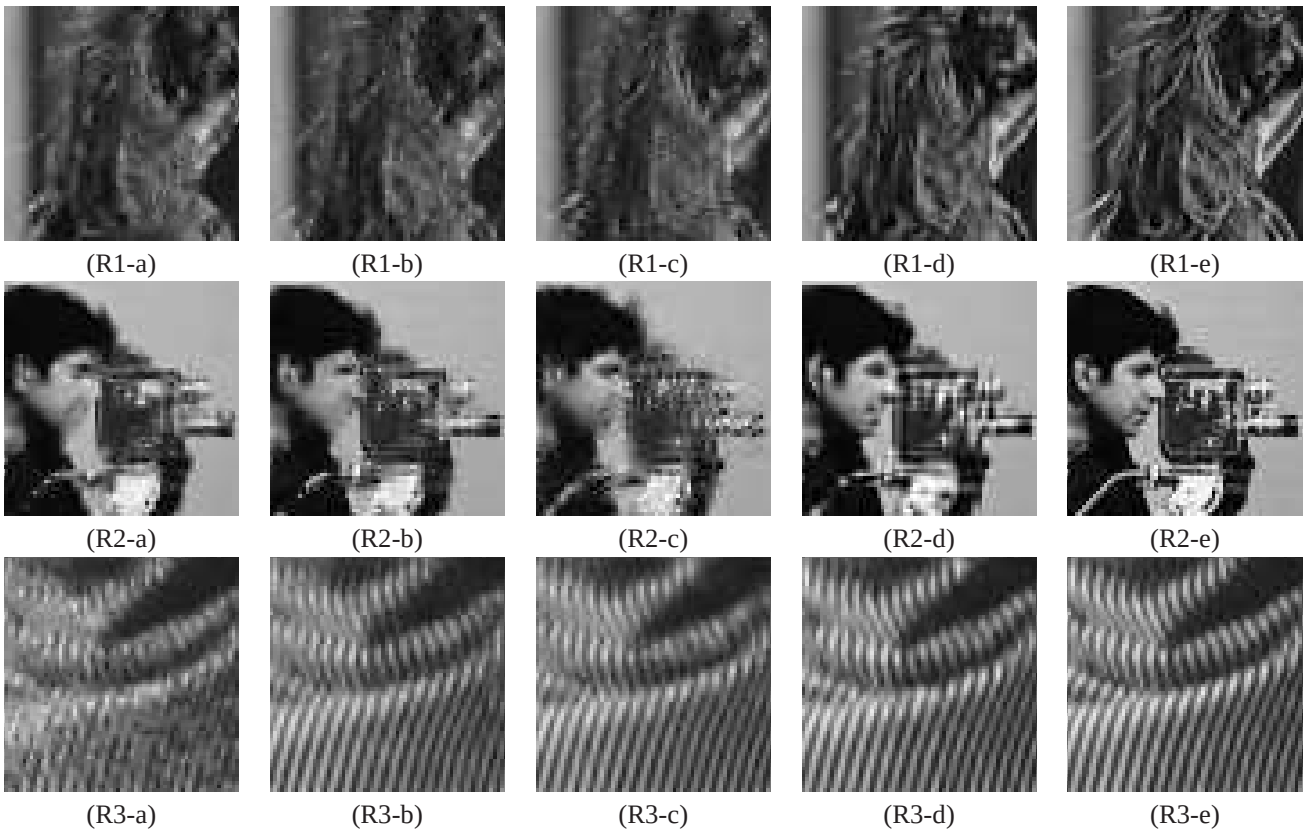

Fig. 7. The results for the zoomed-in portions of the noisy images shown in Figure 6. The first four columns are the inpainted images for the zoomed-in portions by SF, SF-LDCT, MCA, Algorithm 3, respectively. The last column shows the original portions of the images.

Barbara recovered by Algorithm 3 (see Figure 7(R3-d)) is well preserved and visually looks the same as the original one (see Figure 7(R3-e)). Noticeable artifacts are shown in the inpainted images (Figure 7(R3-a)-(R3-c)) with SF, SF-LDCT, and MCA.

C. Effects of The DCT-Haar Wavelets with Different Sizes

The reported performance of Algorithm 3 in the previous two subsections is based on DCT-Haar wavelet from the 7×7 DCT-II matrix. We would like to investigate the effect of changing sizes of the DCT-II matrices on the performance of Algorithm 3. To this end, Algorithm 3 with the DCT-Haar transform matrix W from the DCT-II matrix sizes 5×5, 7×7, 9×9, and 11×11 is applied for inpainting the images in the first row of Figure 2. The corresponding PSNR values of the inpainted images are listed in Table IV. It can be seen that the larger the size of the DCT-II matrix, the higher the PSNR value of the inpainted image. The inpainted images are visually similar and therefore will not be shown here. To avoid compromising the performance and computational complexity of Algorithm 3, the DCT-II matrix size 7×7 is a suitable choice.

TABLE IV
THE PAIR $(\cdot, \cdot)$ REPRESENTS THE PSNR VALUE OF AN INPAINTED IMAGE AND THE CPU TIME (SECONDS) BY ALGORITHM 3 WITH DIFFERENT SIZES OF THE DCT-HAAR SYSTEMS FOR THE TEST IMAGES WITH"TEXT 1".

DCT5	DCT7	DCT9	DCT11	Image
(33.42, 29)	(33.95, 76)	(34.19, 169)	(34.35, 364)	"Lena"
(31.35, 32)	(31.96, 81)	(32.29, 181)	(32.41, 373)	"Cameraman"
(35.36, 26)	(36.98, 64)	(37.59, 153)	(37.96, 314)	"Barbara"

V. CONCLUSIONS

In this paper, we have proposed an image inpainting model which is formulated using the smoothed and weighted ℓ^1 norm of the coefficients of the underlying image and the redundant systems generated by the DCT-Haar multiresolution analysis. We have developed an algorithm based on Beck-Teboulle's method. The weight matrix in the proposed algorithm is updated based on the local information of the coefficients of the solution in iterations. The proposed algorithm outperforms the three state-of-the-art alternatives for various examples in terms of both PSNR values and visual quality of the experimental results. We have claimed that the redundant system generated by the DCT-Haar multiresolution analysis and the resulting inpainting model are particularly suitable for inpainting problems including impulsive noise removal and filling missing information over regions with moderate sizes.

ACKNOWLEDGEMENTS

The authors would like to thank Dr. Jianfeng Cai for providing the source codes of both SF and SF-LDCT, Prof. Elad for making his code MCA available in his website, and the associate editor and the two referees for providing us with valuable comments and insightful suggestions which have brought improvements to several aspects of this manuscript.

The views and conclusions contained herein are those of the authors and should not be interpreted as necessarily representing the official policies or endorsement, either expressed or implied, of the Air Force Research Laboratory or the U.S. Government.

REFERENCES

[1] A. Beck and M. Teboulle, "A fast iterative shrinkage-thresholding algorithm for linear inverse problems," *SIAM Journal on Imaging Sciences*, vol. 2, no. 1, pp. 183–202, 2009.

[2] A. Bovik, *Handbook of Image and Video Processing*. Academic Press, San Diego, 2000.

[3] M. Bertalmio, G. Sapiro, V. Caselles, and C. Ballester, "Image inpainting," in *Proceedings of SIGGRAPH, New Orleans, LA*, 2000, pp. 417–424.

[4] X. Li and Y. Zheng, "Patch-based video processing: a variational bayesian approach," *IEEE Transactions on Circuits and Systems for Video Technology*, vol. 19, no. 1, pp. 27–40, 2009.

[5] C. Ballester, M. Bertalmio, V. Caselles, L. Garrido, A. Marques, and F. Ranchin, "An inpainting-based deinterlacing method," *IEEE Transactions on Image Processing*, vol. 16, no. 10, pp. 2476–2491, 2007.

[6] A. Maalouf, P. Carre, B. Augereau, and C. Fernandez-Maloigne, "A bandelet-based inpainting technique for clouds removal from remotely sensed images," *IEEE Transactions on Geoscience and Remote Sensing*, vol. 47, no. 7, pp. 2363–2371, 2009.

[7] S. Masnou, "Disocclusion: a variational approach using level lines," *IEEE Transactions on Image Processing*, vol. 11, no. 2, pp. 68–76, 2002.

[8] T. F. Chan and J. Shen, "Mathematical models for local nontexture inpaintings," *SIAM Journal on Applied Mathematics*, vol. 62, no. 3, pp. 1019–1043, 2002.

[9] T. F. Chan, S.-H. Kang, and J. Shen, "Euler's elastica and curvature-based image inpainting," *SIAM Journal on Applied Mathematics*, vol. 63, no. 2, pp. 564–592, 2002.

[10] T. F. Chan, J. Shen, and H.-M. Zhou, "Total variation wavelet inpainting," *Journal of Mathematical Imaging and Vision*, vol. 25, no. 1, 2006.

[11] A. Bertozzi, S. Esedoglu, and A. Gillette, "Inpainting of binary images using the cahnchilliard equation," *IEEE Transactions on Image Processing*, vol. 16, no. 1, pp. 285–291, 2007.

[12] J. A. Dobrosotskaya and A. L. Bertozzi, "A wavelet-laplace variational technique for image deconvolution and inpainting," *IEEE Transactions on Image Processing*, vol. 17, no. 5, pp. 657–663, 2008.

[13] M. Ashikhmin, "Synthesizing natural textures," in *Proceedings of the 2001 symposium on Interactive 3D graphics, ACM New York, NY, USA*, 2001, pp. 217–226.

[14] A. Criminisi, P. Perez, and K. Toyama, "Region filling and object removal by exemplar-based inpainting," *IEEE Transactions on Image Processing*, vol. 13, no. 9, pp. 1200–1212, 2004.

[15] N. Komodakis and G. Tziritas, "Image completion using efficient belief propagation via priority scheduling and dynamic pruning," *IEEE Transactions on Image Processing*, vol. 16, no. 11, pp. 2649–2661, 2007.

[16] Y. Wexler, E. Shechtman, and M. Irani, "Space-time completion of video," *IEEE Transactions on Pattern Analysis and Machine Intelligence*, vol. 29, no. 3, pp. 463–476, 2007.

[17] A. Bugeau, M. Bertalmio, V. Caselles, and G. Sapiro, "A comprehensive framework for image inpainting," *IEEE Transactions on Image Processing*, vol. 19, no. 10, pp. 2634–2645, 2010.

[18] M. Elad, J. L. Starck, P. Querre, and D. L. Donoho, "Simultaneous cartoon and texture image inpainting using morphological component analysis (MCA)," *Applied and Computational Harmonic Analysis*, vol. 19, no. 3, pp. 340–358, 2005.

[19] O. G. Guleryuz, "Nonlinear approximation based image recovery using adaptive sparse reconstruction and iterated denoising: part I – theory," *IEEE Transaction on Image Processing*, vol. 15, no. 3, pp. 539–554, 2006.

[20] J. F. Cai, R. H. Chan, and Z. Shen, "A framelet-based image inpainting algorithm," *Applied and Computational Harmonic Analysis*, vol. 24, no. 2, pp. 131–149, 2008.

[21] J. Mairal, M. Elad, and G. Sapiro, "Sparse representation for color image restoration," *IEEE Transactions on Image Processing*, vol. 17, no. 1, pp. 53–69, 2008.

[22] M. J. Fadili, J. L. Starck, and F. Murtagh, "Inpainting and zooming using sparse representations," *The Computer Journal*, vol. 52, no. 1, pp. 64–79, 2009.

[23] J. F. Cai, R. H. Chan, L. Shen, and Z. Shen, "Convergence analysis of tight framelet approach for missing data recovery," *Advances in Computational Mathematics*, vol. 31, no. 1-3, pp. 87–133, 2009.

[24] ——, "Simultaneously inpainting in image and transformed domains," *Numerische Mathematik*, vol. 112, no. 4, pp. 509–533, 2009.

[25] M. Elad, M. A. T. Figueiredo, and Y. Ma, "On the role of sparse and redundant representations in image processing," in *Proceedings of the IEEE*, vol. 98, no. 6, 2010, pp. 972–982.

[26] Z. Xu and J. Sun, "Image inpainting by patch propagation using patch sparsity," *IEEE Transactions on Image Processing*, vol. 19, no. 5, pp. 1153–1165, 2010.

[27] G. Peyre, "Texture synthesis with grouplets," *IEEE Transactions on Pattern Analysis and Machine Intelligence*, vol. 32, no. 4, pp. 733–746, 2010.

[28] J. F. Cai, R. H. Chan, and Z. Shen, "Simultaneous cartoon and texture inpainting," *Inverse Problems and Imaging*, vol. 4, no. 3, pp. 379–395, 2010.

[29] N. Ahmed and K. R. Rao, *Orthogonal Transforms for Digital Signal Processing*. New York: Springer-Verlag, 1975.

[30] E. J. Candes, M. B. Wakin, and S. P. Boyd, "Enhancing sparsity by reweighted ℓ^1 minimization," *Journal of Fourier Analysis and Applications*, vol. 14, no. 5, pp. 877–905, 2008.

[31] R. H. Chan, L. Shen, and Z. Shen, "A framelet-based approach for image inpainting," The Chinese University of Hong Kong, Tech. Rep. 2005-4, Feb. 2005.

[32] J.-J. Moreau, "Proximité et dualité dans un espace hilbertien," *Bull. Soc. Math. France*, vol. 93, pp. 273–299, 1965.

[33] Q. Lian, L. Shen, Y. Xu, and L. Yang, "Filters of wavelets on invariant sets for image denoising," *Applicable Analysis*, vol. 90, no. 8, pp. 1299–1322, 2011.

[34] E. J. Candes, J. Romberg, and T. Tao, "Stable signal recovery from incomplete and inaccurate measurements," *Communications on Pure and Applied Mathematics,*, vol. 59, no. 8, pp. 1207–1223, 2006.

[35] ——, "Robust uncertainty principles: exact signal reconstruction from highly incomplete frequency information," *IEEE Transactions on Information Theory*, vol. 52, no. 2, pp. 489–509, 2006.

[36] M. Lustig, D. L. Donoho, J. Santos, and J. Pauly, "Compressed sensing MRI," *IEEE Signal Processing Magazine*, vol. 25, no. 2, pp. 72–82, 2008.

[37] I. Daubechies, R. DeVore, M. Fornasier, and C. Gunturk, "Iteratively reweighted least squares minimization for sparse recovery," *Communications on Pure and Applied Mathematics,*, vol. 63, no. 1, pp. 1–38, 2010.

[38] H. L. Bauschke and P. L. Combettes, *Convex Analysis and Monotone Operator Theory in Hilbert Spaces*, ser. AMS Books in Mathematics. Springer, New York, 2011.

[39] Y. R. Li, L. Shen, D. Q. Dai, and B. W. Suter, "Framelet algorithms for de-blurring images corrupted by impulse plus gaussian noise," *IEEE Transactions on Image Processing*, vol. 20, no. 7, pp. 1822–1837, 2011.

[40] Y. R. Li, D. Q. Dai, and L. Shen, "Multiframe super-resolution reconstruction using sparse directional regularization," *IEEE Transactions on Circuits and Systems for Video Technology*, vol. 20, no. 7, pp. 945–956, 2010.

[41] R. Gonzalez and R. Woods, *Digital Image Processing*. Addison-Wesley, Boston, MA, 1993.